Comment on amt-2022-247

Anonymous Referee # 4

Referee comment RC3 on "Retrieval of Terahertz Ice Cloud Properties from airborne measurements based on the irregularly shaped Voronoi ice scattering models" by Ming Li et al.

General comments

This study implements Voronoi and spherical ice crystal models in observed brightness temperatures at 380, 640 and 874 GHz to retrieve Ice water path(IWP) and effective particle radius (Re). Authors show that Voronoi model can better reproduce results compared to previous 'standard' values. I think such result is obvious and can be easily predicated as simple spherical model is less adequate for irregular-shaped ice particles, but authors showed it quantitatively. In my opinion, there exist mistakes/incompleteness in English language, methodology, and scientific discussions, as outlined in specific comments below. Authors are suggested to improve the manuscript by considering the comments given below as well as by carefully improving the English writing/expression.

Response: Thank you very much for your significant comments.

Specific comments

1. Line 19: '.. we completed the..'--> completed is what sense? rewrite it.

Response: We have rewritten it as follows: ".. we developed the Voronoi ..".

2. Line 48 : '..signfinifiantly developed...': rewrite the sentence.

Response: We have rewritten this sentence as follows: "Currently, large amounts of passive sensors (visible, infrared and microwave detectors) have been developed and related ice cloud retrieval algorithms have been reported in substantial literature (Nakajima and King, 1990; Nakajima et al., 1991, 2019; Nakajima and Nakajima, 1995; Platnick et al., 2003, 2017; Fox et al., 2019; Brath et al., 2018).".

3. Line 132: What is 'CoSSIR-MCBI' algorithm? A brief description is important with relevant references.

Response: According to the comments, we have illustrated the definition of the "CoSSIR-MCBI" abbreviation on lines 73 - 76 as follows: "Evans et al. (2002) developed a Monte Carlo Bayesian Integration (MCBI) algorithm to retrieve ice clouds' IWP and median mass diameter (D_{me}) from simulated SWCIR brightness temperatures. Then, Evans et al. (2005) applied the MCBI method to retrieve IWP and D_{me} using the CoSSIR brightness temperatures (referred to as the CoSSIR-MCBI hereafter).".

4. Lines 140-143: Specify ice particle sizes either in table or describe size interval in the text. Provide same information for the 20 wavelengths mentioned here.

Response: According to the comments, we have added one table (Table 1) to list the 31 ice particle sizes and 20 wavelengths contained in the single-scattering property database of the Voronoi ICS model. Table 1 is shown below. We have also modified the corresponding descriptions on lines 140-142 as follows: "For the Voronoi ICS model, the single-scattering property database contains 31 ice particle sizes ranging from 0.25 to 9300 μm and covers 20 terahertz channels with frequencies ranging from 10 to 874 GHz, corresponding to wavelengths from 0.03 to 3cm (see Table 1).".

Table 1. The 20 frequency channels and 31 maximum dimensions of ice particles included in the single-scattering property database of the Voronoi ICS model.

Maximum dimension (μm)	Frequency (GHz)	Wavelength (cm)
0.400E+00	0.10000E+02	0.29979E+01
0.100E+01	0.15000E+02	0.19986E+01
0.200E+01	0.18700E+02	0.16032E+01
0.300E+01	0.23800E+02	0.12596E+01
0.500E+01	0.31400E+02	0.95475E+00
0.750E+01	0.35000E+02	0.85655E+00
0.150E+02	0.50300E+02	0.59601E+00
0.250E+02	0.53750E+02	0.55775E+00
0.350E+02	0.55000E+02	0.54508E+00
0.450E+02	0.89000E+02	0.33685E+00

0.600E+02	0.94000E+02	0.31893E+00
0.700E+02	0.11875E+03	0.25246E+00
0.147E+03	0.16550E+03	0.18114E+00
0.225E+03	0.18331E+03	0.16354E+00
0.314E+03	0.22900E+03	0.13091E+00
0.419E+03	0.24300E+03	0.12337E+00
0.500E+03	0.32500E+03	0.92244E-01
0.623E+03	0.44800E+03	0.66918E-01
0.752E+03	0.66400E+03	0.45150E-01
0.867E+03	0.87400E+03	0.34301E-01
0.964E+03		
0.108E+04		
0.140E+04		
0.175E+04		
0.256E+04		
0.350E+04		
0.500E+04		
0.750E+04		
0.100E+05		
0.120E+05		
0.150E+05		

5. Line 149: Specify what refractive index values are used for ice particles here. Give a reference.

Response: According to the comments, we have added specifications and the reference on lines 148-149 as follows: "Calculations of the single-scattering property utilize the real and imaginary parts of ice from the newest library of the refractive index provided by Warren and Brandt (2008).".

6. I think Figure 1 is confusing. Either make Figure 1 clear or remove it and describe the mythology clearly in the text.
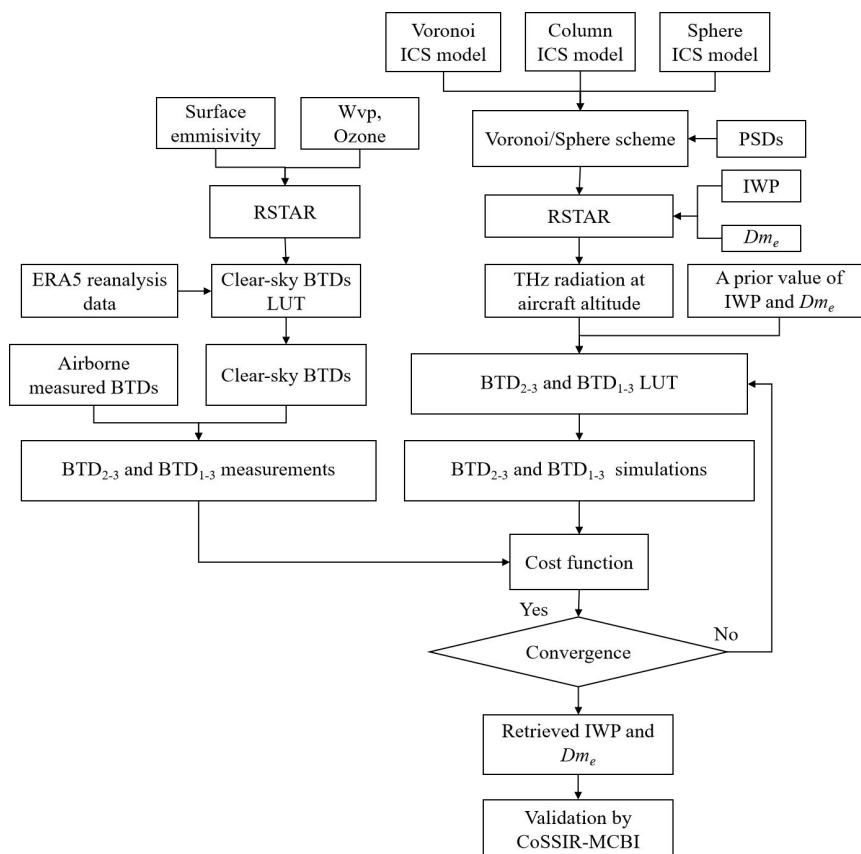
Figure 1: The overall flowchart of the retrieval of the IWP and D_{me} of ice clouds based on the Voronoi, Sphere and Column ICS models.

7. Line 179: I do not understand how clear sky days are selected here. Are they before and/or after the cloudy sky days or average of certain week (or month etc.)?

Response: Here we simulated a clear-sky observed scenario based on the radiative transfer model. We are aimed to construct a clear-sky look-up table with different inputs of water vapour and ozone columns. This clear-sky look-up table is used later in the retrieval process that follows.

8. Lines 188-189: 'statistical multiple linear regression method': Write a few lines to clarify it. For example, what are dependent and independent variables in this method?

Response: According to the comments, we have added more illustrations of the "statistical multiple linear regression method" on lines 188-191 as follows: "Due to

the different definitions of R_e and D_{me}, a transformation of the particle size descriptors is necessary. A statistical multiple linear regression was used in the transformation. Firstly, the ice particle number concentration of ice clouds was specified. A total of 14,408 groups of PSDs from aircraft observation sampling data were selected. The equivalent-volume sphere's particle radius, maximum particle dimension and mass were used to integrate over 14,408 PSDs. Then 14,408 groups of R_e and D_{me} were implemented. Finally, we build a relationship between the R_e and D_{me} and coefficients can be obtained by numerical fitting and provided as input. We regard the R_e and D_{me} as independent and dependent variables, respectively. Therefore, D_{me} can be calculated from the coefficients.".

9. Line 199: A reference for Eq. (3) is required.

Response: According to the comments, we have added a reference for Eq. (3) as follows: ".. we adopt the gamma distribution form following Heymsfield et al. (2013) as follows ..".

10. Lines214-219: Please specify the coefficient terms either in table or in text.

Response: According to the comments, we have added four tables (Table A.1-A.4) listing the coefficient terms of Eq. (9)-(12) as shown below. We have added descriptions as follows: "Values of the above coefficients for Voronoi scheme are listed in appendix A (Tables A.1, A.2, A.3, and A.4).".

Table A.1

Coefficients in the fitting of terahertz mass extinction coefficients (m^2 /g).

Frequency (GHz)	a_0 (m^2/g)	a_1 (m^3/g)
325	7.0891e-01	-1.6965e+01
448	2.1347e+00	-5.0405e+01
664	7.5009e+00	-1.6770e+02
874	1.5790e+01	-3.2850e+02

Table A.2

Coefficients in the fitting of terahertz single-scattering albedo.

Frequency (GHz)	b_0	b_1	b_2	b_3
325	-3.1317e-01	2.7448e-02	-2.0449e-04	5.0815e-07
448	-2.3947e-01	2.9461e-02	-2.4145e-04	6.4366e-07
664	-8.2857e-02	2.7985e-02	-2.4357e-04	6.7691e-07
874	4.7425e-02	2.5164e-02	-2.2395e-04	6.3152e-07

Table A.3

Coefficients in the fitting of terahertz asymmetry factor.

Frequency (GHz)	c_0	c_1	c_2	c_3
325	2.2045e-02	-8.2487e-04	2.5764e-05	-4.7767e-08
448	1.0168e-02	-5.1223e-05	3.0599e-05	-8.0591e-08
664	-4.4704e-02	3.5331e-03	1.2997e-05	-7.2297e-08
874	-1.1685e-01	8.8403e-03	-3.0410e-05	2.6790e-08

Table A.4

Coefficients in the fitting of terahertz mass-averaged absorption coefficients (m^2/g).

Frequency (GHz)	d_0 (m^2/g)	d_1 (m/g)	d_2 (1/g)	d_3 (m^{-1}/g)
325	4.4262e-02	1.5585e-04	9.6647e-07	-5.1271e-09
448	8.2110e-02	5.0544e-04	2.0336e-06	-1.2945e-08
664	1.6909e-01	2.4299e-03	1.2784e-06	-3.3930e-08
874	2.6509e-01	7.6295e-03	-1.4488e-05	-3.9275e-08

11. L222: Is BTD_{1-3} is same to BTD_{1-2}-BTD_{2-3} ? If so, better to write BTD_{1-3} instead of BTD_{1-2}-BTD_{2-3}.

Response: According to the comments, we have replaced the BTD_{1-2}-BTD_{2-3} with BTD_{1-3} and have unified them in the revised manuscript. The relevant descriptions are shown below.

Lines 221-223: "The difference between the 640 GHz BTD and the 874 GHz BTD is simplified to BTD_{2-3}. And the difference between the 380 GHz BTD and the 640 GHz

BTD is simplified to BTD_{1-2}. We named the difference between the BTD_{1-2} and BTD_{2-3} as BTD_{1-3}."

12. Lines 227-229: I think BTD depends strongly on cloud top temperature as well as surface temperature along with cloud properties. Since they are fixed here, errors are expected in retrieved values. Can authors provide error ranges in retrieved parameters due to such assumptions? If possible, authors are suggested to use actual data from cloud top and surface temperatures rather than assumptions.

Response: Thanks for the comments. For large particles (SZP>1), the scattering is mainly Mie scattering, and the single scattering albedo is close to 1 (Figure 1). Hence, ice particle scattering plays a leading role. Since the radiation is mainly scattered by ice crystal particles, the absorption effects and emission effects are small, and the BTD THz radiation at the top of the atmosphere is almost independent of cloud top temperature.

For the error caused by the surface temperature assumptions, the clear-sky atmospheric optical thickness for the 0.3-3 Thz is large as shown in Figure 2. Thus most of the radiation emitted by the surface temperature is absorbed by the lower layer of water vapor and ozone. Furthermore, there is a lack of actual surface temperature data synchronized with the airborne measurement track. Furthermore, the reanalysis data such as ERA5 with coarse spatial resolution will introduce new errors to retrieval results.
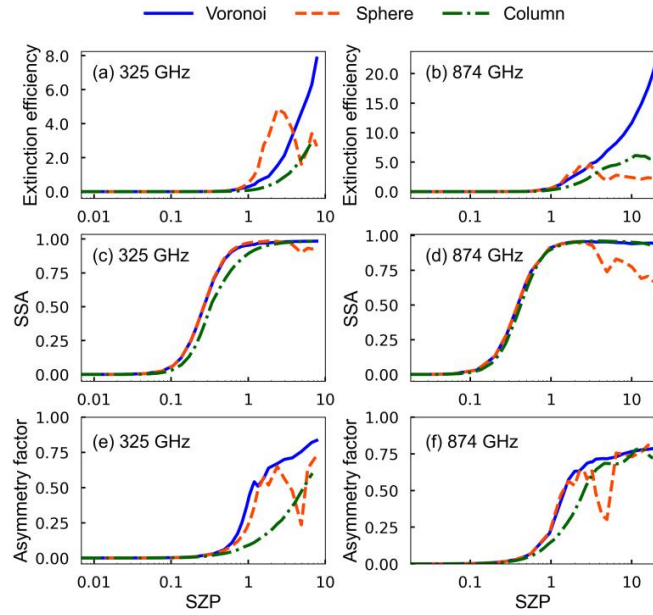
Figure 1: The extinction efficiency, single-scattering albedo and asymmetry factor as functions of the SZP for the Voronoi (blue solid line), Sphere (red dashed line) and Column (green dashed line) ICS models in the (a, c, e) 325 and (b, d, f) 874 GHz frequencies.
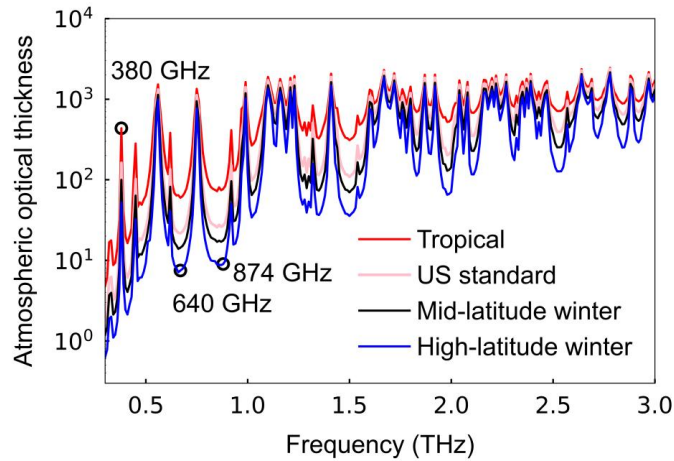

Figure 2. The spectral variations of the clear-sky atmospheric optical thickness under four atmospheric conditions.

13. A theoretical perspective should be given for using BTD_{2-3} and $BTD_{1-2} - BTD_{2-3}$ in Eq. 4. (Why these two are important in cloud properties retrieval among several possible combinations of three wavelengths). Further, there should be an error term in Eq. 13. It is further necessary to describe in detail about the methodology. For example, what are the convergence criteria, how the initial values are determined, and

how measurement errors can affect the retrieved values etc.

Response: Thanks for the comments. For the first question, the basis of using the combination of the BTD_{2-3} and BTD_{1-2} -BTD_{2-3} is as follows: The 380 GHz is the atmospheric absorption peak, while 640 and 874 GHz are the atmospheric windows as shown in Figure 2 below. Therefore, both the 640 and 874 GHz brightness temperature are affected by ice clouds, while the brightness temperature of 380 GHz is insensitive to ice cloud microphysical properties. Hence, the 380 minus 640 GHz brightness temperature differences (BTD_{1-2}) can highlight the brightness temperature depression caused by ice clouds. And the 640 minus 874 GHz brightness temperature differences (BTD_{2-3}) can reflect the difference in the scattering properties of differently shaped ice clouds. This is helpful to study the role of different ice crystal shapes. The differences between 640 and 874 GHz also can offset the regional errors due to different latitudes, atmospheric profiles and atmospheric states. In summary, The BTD_{2-3} and BTD_{1-2} -BTD_{2-3} combination can integrate the information of three frequencies and show the sensitivity to ice clouds, eliminating the impacts of different atmospheric profiles and conditions.
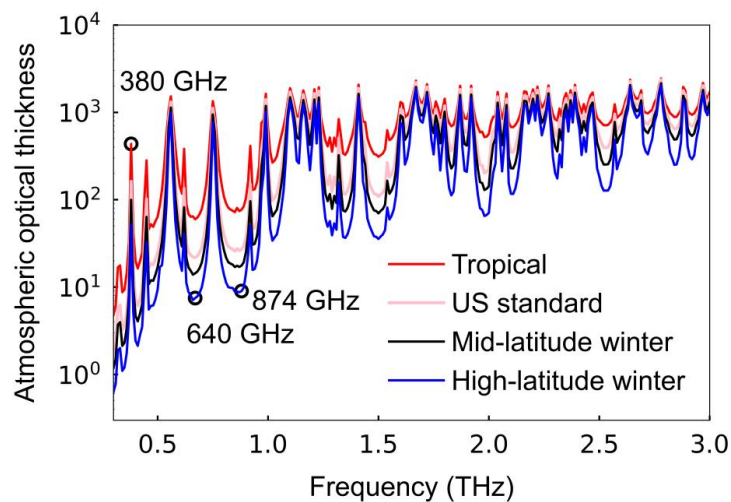

Figure 2. The spectral variations of the clear-sky atmospheric optical thickness under four atmospheric conditions.

For the second question, we have modified the Eq. (13)-(14) and added the detailed method as shown below.

"

$$Y = F(X) + \epsilon \ , \qquad\qquad\qquad\qquad (13)$$

$$X = \begin{pmatrix} IWP, \\ D_{me} \end{pmatrix} \ , \ F(X) = \begin{pmatrix} BTD_{2-3}, \\ BTD_{1-2} - BTD_{2-3} \end{pmatrix}, \qquad (14)$$

where X is the vector-matrix composed of the variables of the IWP and D_{me} to be solved. Y is the vector composed of the two BTDs and the uncertainty vector. The vector ϵ represents the uncertainties that are attached to the measurements (i.e. instrumental accuracy) and to the radiative transfer forward model (i.e.approximation errors in the radiative transfer model). Following Marks and Rodgers (1993), a good convergence can be obtained when the value of the cost function is lower than the size of the measurement vector. Since there is no robust a priori for IWP and D_{me}, we selected an average value as the initial value for a priori value of the IWP and D_{me}."

14. Line 250: Since the x-axis is size parameter (not radius), it is difficult to understand where 120um exist. Either rewrite the text or make Figure 2 clear by adding additional x-axis.

Response: According to the comments, we have rewritten the text as follows: "For small ice particles with SZPs less than 1, the single-scattering properties are small and barely influenced by the shape of ice particles.".

15. Lines 250-254: Why large difference exists for large sized particles in Figure 2 remains undiscussed.

Response: Thanks for the comments, we have added discussions on lines 254-256 as follows: "As ice particle size increases, scattering is predominantly Mie scattering and sensitivity of the single-scattering properties to the ice crystal habits becomes pronounced, so that ice crystal shape contributes to the large differences for large particle sizes. ".

16. Lines 261-264: What could be the plausible reasons for such results for relatively larger particles?

Response: We have added reasons on lines 261-264 as shown below.

Lines 273-277: "On the one hand, the higher extinction efficiency and single-scattering albedo of the Voronoi ICS model for large particles are possibly due to the multifaceted shapes of the Voronoi ICS model, which can result in significant

side and backward scattering and increase the scattered energy. On the other hand, for large particles, the higher asymmetry factor of the Voronoi ICS model is possibly because the scattered energy is dominated by diffraction. The diffracted energy is concentrated in the forward direction, leading to a large asymmetry factor."

17. I do not understand why BTD2 is shown in Figure 6 as it is not used in the retrieval (see Eq. 4).

Response: Thanks for the comments. We have replaced BTD_2 with BTD_{2-3} in Figures 6 and 7, as shown below.
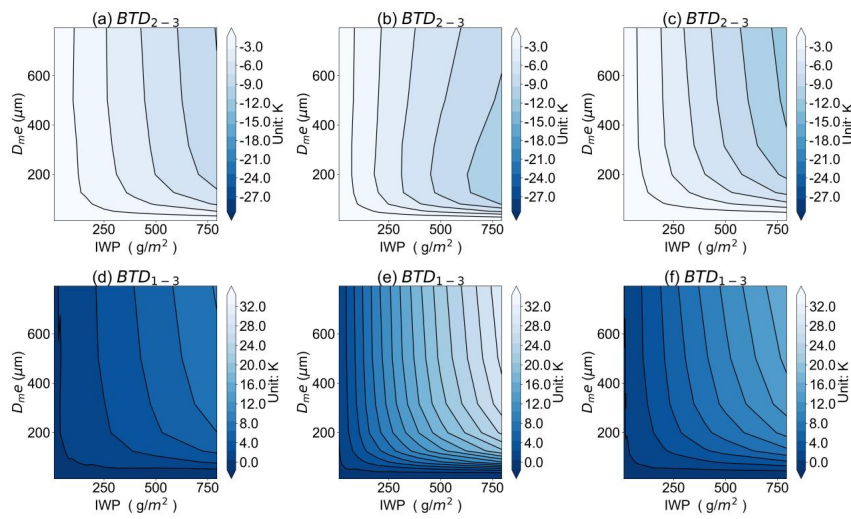

Figure 6: The BTD_{2-3} and BTD_{1-3} for the (a, d) Voronoi, (b, e) Sphere and (c, f) Column ICS models as functions of the IWP and D_{me}, respectively.
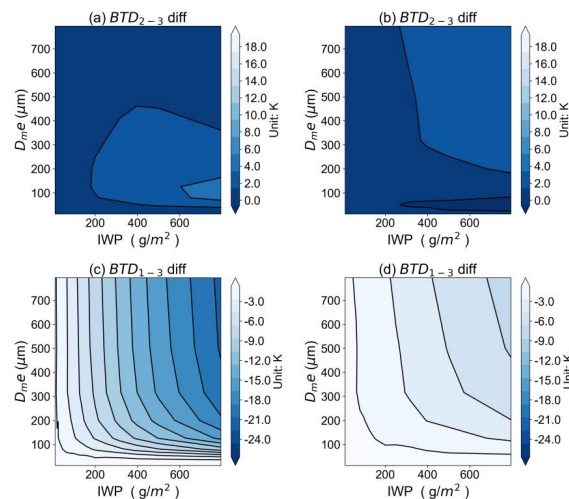

Figure 7: The difference of BTD_{2-3} and BTD_{1-3} for the (a, c) Voronoi minus Sphere ICS models and (b, d) Voronoi minus Column ICS models as functions of the IWP and D_{me}, respectively.

18. Please make Figure 7 easy to understand. For example, indicate the values of IWP and Re with dots (e.g., Nakajima and King plot). As there are overlapping lines in Figure 7, how cloud properties are retrieved if data fall under such overlapping lines?

Response: According to the comments, we have indicated the values of IWP and Re with dots. When BTD_{2-3} and BTD_{1-3} data fall under such overlapping lines, this overlapping region can lead to obtaining the same IWP and D_{me} when searching the look-up table. That is why the "horizontal line" problem occurs for $D_{me} < 40$ μm and $D_{me} > 40$ μm. This is one of the limitations of our method, which is more applicable for moderate ice particles. And we will improve our retrieval algorithm in the next step.
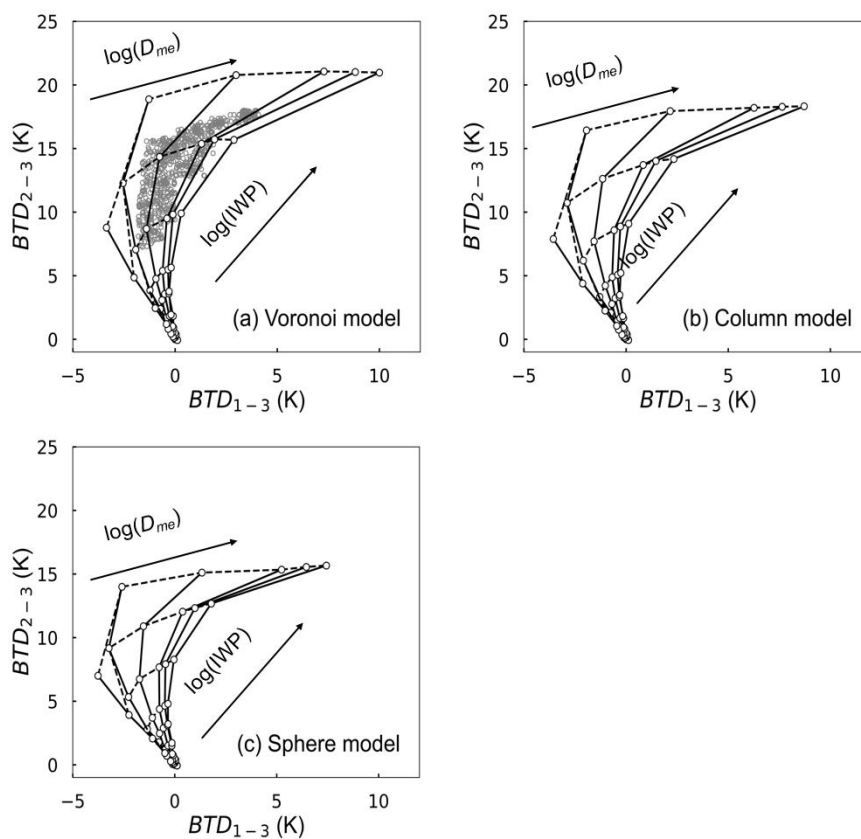

Figure 7: The LUT of BTD_{2-3} and BTD_{1-3} for the (a) Voronoi, (b) Column and (c) Sphere ICS models varying with the logarithm of IWP and D_{me}. Grey dots in circles represent the randomly generated 2000 test data from RSTAR model.

Reference

Brath, M., Fox, S., Eriksson, P., Harlow, C., Burgdorf, M., and Buehler, S.: Retrieval of an ice water path over the ocean from ISMAR and MARSS millimeter and submillimeter brightness temperatures, Atmospheric Measurement Techniques, 11, 611-632, doi:10.5194/amt-11-611-2018, 2018.

Evans, K., Wang, J., Racette, P., Heymsfield, G., and Li, L.: Ice Cloud Retrievals and Analysis with the Compact Scanning Submillimeter Imaging Radiometer and the Cloud Radar System during CRYSTAL FACE, Journal of Applied Meteorology - J APPL METEOROL, 44, 839-859, doi:10.1175/JAM2250.1, 2005.

Evans, K. F., Walter, S. J., Heymsfield, A. J., and McFarquhar, G. M.: Submillimeter-Wave Cloud Ice Radiometer: Simulations of retrieval algorithm performance, Journal of Geophysical Research: Atmospheres, 107, AAC 2-1-AAC 2-21, doi:10.1029/2001JD000709, 2002.

Fox, S., Mendrok, J., Eriksson, P., Ekelund, R., amp, apos, Shea, S., Bower, K., Baran, A., Harlow, C., and Pickering, J.: Airborne validation of radiative transfer modelling of ice clouds at millimetre and sub-millimetre wavelengths, Atmospheric Measurement Techniques, 12, 1599-1617, doi:10.5194/amt-12-1599-2019, 2019.

Heymsfield, A. J., Schmitt, C., and Bansemer, A.: Ice Cloud Particle Size Distributions and Pressure-Dependent Terminal Velocities from In Situ Observations at Temperatures from 0 degrees to-86 degrees C, J Atmos Sci, 70, 4123-4154, 2013.

Marks, C. and Rodgers, C.: A retrieval method for atmospheric composition from limb emission measurements, Journal of Geophysical Research, 981, 10.1029/93JD01195, 1993.

Nakajima, T. and King, M. D.: Determination of the Optical-Thickness and Effective Particle Radius of Clouds from Reflected Solar-Radiation Measurements .1. Theory, J Atmos Sci, 47, 1878-1893, doi:10.1175/1520-0469(1990)047<1878:Dotota>2.0.Co;2, 1990.

Nakajima, T., King, M. D., Spinhirne, J. D., and Radke, L. F.: Determination of the Optical-Thickness and Effective Particle Radius of Clouds from Reflected Solar-Radiation Measurements .2. Marine Stratocumulus Observations, J Atmos Sci, 48, 728-750, doi:10.1175/1520-0469(1991)048<0728:Dotota>2.0.Co;2, 1991.

Nakajima, T. Y. and Nakajima, T.: Wide-area determination of cloud microphysical properties from NOAA AVHRR measurements for FIRE and ASTEX regions, J Atmos Sci, 52, 4043-4059, doi:10.1175/1520-0469(1995)052<4043:Wadocm>2.0.Co;2, 1995.

Nakajima, T. Y., Ishida, H., Nagao, T. M., Hori, M., Letu, H., Higuchi, R., Tamaru, N., Imoto, N., and Yamazaki, A.: Theoretical basis of the algorithms and early phase results of the GCOM-C (Shikisai) SGLI cloud products, Prog Earth Planet Sc, 6, doi:10.1186/s40645-019-0295-9, 2019.

Platnick, S., King, M. D., Ackerman, S. A., Menzel, W. P., Baum, B. A., Riedi, J. C.,

and Frey, R. A.: The MODIS cloud products: algorithms and examples from Terra, IEEE Transactions on Geoscience & Remote Sensing, 41, 459-473, doi:10.1109/TGRS.2002.808301, 2003.

Platnick, S., Meyer, K. G., King, M. D., Wind, G., Amarasinghe, N., Marchant, B., Arnold, G. T., Zhang, Z. B., Hubanks, P. A., Holz, R. E., Yang, P., Ridgway, W. L., and Riedi, J.: The MODIS Cloud Optical and Microphysical Products: Collection 6 Updates and Examples From Terra and Aqua, Ieee T Geosci Remote, 55, 502-525, doi:10.1109/Tgrs.2016.2610522, 2017.

Warren, S. G. and Brandt, R. E.: Optical constants of ice from the ultraviolet to the microwave: A revised compilation, J Geophys Res-Atmos, 113, 2008.